



ARTICLE

Highly Efficient Adsorption of P-Xylene from Aqueous Solutions by Hierarchical Nanoporous Biochar Derived from Crab Shell

Yingna Chen¹, Hailong Zhang², Jian Guo¹, Lu Cai³, Yaning Wang⁴, Xinxin Yao⁵, Wendong Song⁶ and Lili Ji^{4,*}

¹College of Food and Medical, Zhejiang Ocean University, Zhoushan, 316022, China

²National-Local Joint Engineering Laboratory of Harbor Oil & Gas Storage & Transportation Technology, School of Petrochemical Engineering & Environment, Zhejiang Ocean University, Zhoushan, 316022, China

³Donghai Science and Technology College, Zhejiang Ocean University, Zhoushan, 316000, China

⁴Institute of Innovation & Application, Zhejiang Ocean University, Zhoushan, 316022, China

⁵College of Naval Architecture and Mechanical-Electrical Engineering, Zhejiang Ocean University, Zhoushan, 316022, China

⁶College of Petrochemical and Energy Engineering, Zhejiang Ocean University, Zhoushan, 316022, China

*Corresponding Author: Lili Ji. Email: jll-gb@163.com

Received: 24 January 2021 Accepted: 16 March 2021

ABSTRACT

The global consumption of p-xylene (PX) for the production of polymers has raised serious concerns about its impact on the environment. As various reports have shown the risks that PX could pose to human health, research into cost-effective remedial methods to remove PX from the environment has gained attraction. In this work, a hierarchical porous crab shell biochar (KCS) was synthesized, characterized, and evaluated for its efficiency to remove PX from aqueous solution. The characterizations of KCS, including the porous structure, surface functional group, phase structure, and surface morphology, were discussed by N₂ adsorption-desorption, FTIR, XRD, and SEM. Batch adsorption experiments showed that the maximum adsorption capacity of PX on KCS was 393 mg/g within 5 min, larger than most biological/biomass materials, mainly due to the higher specific surface area of 2046 m²/g, and abundant lipophilic functional groups. Subsequent adsorption kinetics study indicated a pseudo-second-order model which implied that the adsorption of PX was due to chemisorption. Thermodynamic parameters showed that the values of ΔH° and ΔG° were both negative, indicating that the PX adsorption process on KCS was spontaneous and exothermic. The performance of KCS in delivering a cost-effective, fast, and efficient solution for the removal of PX from aqueous solution would greatly benefit current environmental remediation efforts.

KEYWORDS

Crab shell; porous biochar; p-xylene; adsorption; wastewater

1 Introduction

In the past few decades, the demand for xylene (PX) has increased exponentially owing to its widespread application as a chemical feedstock for the production of various polymers [1]. Only as a raw material of polyethylene terephthalate (PET) [2], its global demand has reached 45 million tons in 2016 [3] and was



expected to rise further. Due to its widespread usage, it potentially can leak into the soil, surface water, and groundwater, hence raising environmental concerns [4,5]. It may also pose a risk to human health, causing kidney, liver, and nervous system damage [6]. Therefore, the removal of these hazardous and harmful compounds from wastewater is of great significance to resolve the issues of environmental organic pollutants. Several methods have been reported for its removal, such as non-thermal plasma [7], air sparging [8], chemical oxidation [9,10], and adsorption [11,12]. Among these solutions, adsorption was one of the most attractive methods due to its low cost, high efficiency, and superior stability [13,14].

Biochar has been recently identified as a novel material with high adsorption capacity and demonstrated high efficiency for the removal of organic [15–17], inorganic [18–20], and biological contaminants [2,21] from wastewater. This was attributed to its good electrical conductivity, stable chemical properties, high specific surface areas, and controllable pore structures [22]. Biochar was usually produced from biomass, and crustacean waste was seen as a viable source since it is one of the most abundant biomass in nature. As an abundant and cheap food waste, crab shells can be obtained readily from Zhoushan local seafood market. Previously, crustacean waste has been utilised as a raw material for the production of chitin and chitosan [23] as well as electrode materials for supercapacitors [24]. Oxidation was the method to introduce the functional groups, change the surface area, surface charge, and hydrophobicity [25–27]. Arshadi et al reported that the presence of the free carboxyl groups of citric acid raises the density of electron donating groups, and it was the responsible for higher uptake of BTEX [28]. Similarly, Cai et al showed that crab shell treated with potassium hydroxide was found to exhibit mesoporous structures and contained hydroxyl and carboxyl functional groups, leading to its high adsorption capacity for diesel oil [29]. The purpose of this study was to examine the feasibility of using crab shell waste as a novel p-xylene adsorbent. In addition, crab shell-based biochar can not only make use of the superior natural structure of crab shells, but also effectively solve the environmental pollution caused by a large number of discarded crab shells. However, to our best of knowledge, the application of crab shell biochar for the adsorption of PX has not yet been reported.

In this work, crab shell biochar treated with potassium hydroxide was studied for its performance for the removal of PX from aqueous solution. The as-prepared biochar was characterized by scanning electron microscopy (SEM), X-ray powder diffraction (XRD), Fourier transformed infrared (FTIR) and its surface area was determined using the Brunauer–Emmett–Teller (BET) method. Batch adsorption experiments were also carried out to investigate the effects of adsorption time and pH on the efficiency of PX removal from aqueous solution. Adsorption kinetics study of PX was performed using pseudo-first order, pseudo-second order, and intraparticle diffusion models. Adsorption isotherm of PX was investigated using Langmuir, Freundlich, and Dubinin-Radushkevich isotherm models. Lastly, the amount of PX adsorbed at equilibrium was also measured at different adsorption temperatures, and the thermodynamic parameters of the adsorption process were investigated.

2 Materials and Methods

2.1 Materials

Crab shell was purchased from a local seafood market in Zhoushan, washed repeatedly with distilled water to eliminate surface impurities, and dried at 105°C for 12 h in the oven. HCl, KOH and PX were obtained from Sinopharm Chemical Reagent Co., Ltd., Shanghai, China. The chemicals used in this study were analytical grade and were used at the time of reception without further purification unless specified otherwise.

2.2 Preparation of Activated Crab Shell Powder

Crab shell (30 g) was immersed in 2 mg/L HCl solution for 12 h to remove calcium carbonate. The crab shell was subsequently rinsed with distilled water to remove HCl and salts remaining on the surface and dried in the oven at 80°C overnight. The pretreated crab shell (CS) was then crushed into powder, and carbonized

in a tubular furnace under nitrogen flow (200 mL/min) with a temperature ramping rate of 10°C/min, and held at 700°C for 120 min.

Then, the pre-carbonized crab shell was ground into a powder and used in the subsequent activation experiments. The pre-carbonized CS was mixed with KOH (CS weight/KOH weight = 2.5:1) and activated in the tubular furnace under nitrogen flow (200 mL/min) with a temperature ramping rate of 10°C/min, and held at 800°C for 60 min. After cooling down to room temperature, the obtained activated biochar was washed with a large amount of distilled water until the filtrate was neutral, and further dried in an oven at 80°C overnight. It was then stored in an air-tight sample vessel. The as-prepared activated biochar was denoted as KOH activated crab shell (KCS). The activation mechanism was referred to in the following reactions Eqs. (1)–(4) [30]. Finally, we were obtained 3.15 g KCS and the yield of biochar was 10.5%.



2.3 Characterization of CS and KCS

N₂ adsorption isotherm was performed on the static capacity adsorption analyzer (NOVA 2200e, Quanta chrome, Florida, USA). Surface groups were characterized by Fourier-transform infrared (FTIR, IRAffinity-1S, Tokyo, Japan) in the range of 400–4000 cm⁻¹. X-ray diffraction (XRD) patterns of samples were recorded on an Ultima IV X-ray Diffractometer (XRD, DX-2700, Liaoning, China) in the range of 2θ from 10° to 80°. Scanning electron microscopy was conducted to visualize the microstructure and morphology of the samples (SEM, Hitachi S-4800, Tokyo, Japan).

2.4 Batch Adsorption of PX

0.01 g KCS and CS were respectively added into 50 mL PX aqueous solution with the concentration range of 10, 20, 40, 60, 80, 100 mg/L for adsorption to analyze the impact of initial concentration. The solution pH was adjusted from 5.0 to 9.0, and the adsorption reaction time is from 5 to 120 min. Centrifuge the mixed solution at a speed of 4000 r/min for 5 min, then sample the transparent liquid on the top and measure its adsorption value (UV 2600, Shimadzu, Shanghai, China). Calculate the concentration of PX in the adsorbent based on the absorption value, and further calculate the amount of PX adsorbed by CS or KCS.

2.5 Study on Adsorption Kinetics and Thermodynamics

To investigate the kinetics of PX adsorption, 0.01 g of KCS was added into 50 mL of 80 mg/L PX solution at time intervals from 0 to 120 min. For adsorption isotherms data, 50 mL PX with different initial concentration (10, 20, 40, 60, 80, 100 mg/L) was treated with 0.01 g KCS. Initial and final concentrations of PX were analyzed using a UV–Vis spectrophotometer (UV 2600, Shimadzu, Shanghai). The thermodynamic behavior was investigated at 25, 30, 35, and 40°C by using 0.01 g KCS and 50 mL 80 mg/L PX solution (pH = 7).

2.6 Data Analysis

2.6.1 Adsorption Calculation

The adsorption amount q_t (mg/g) and removal efficiency R (%) of PX were respectively calculated according to the formula below:

$$q_t = \frac{(C_0 - C_t)V}{m} \quad (5)$$

$$R = \left(\frac{C_0 - C_t}{C_0} \right) \times 100 \quad (6)$$

where q_t (mg/g) was the amount of PX taken up by the adsorbents, C_0 (mg/L) and C_t (mg/L) represented the initial concentration and the concentration at some reaction time point, V was the volume of the solution (L), and m (g) is the weight of KCS and CS.

2.6.2 Adsorption Kinetics Study

Adsorption kinetics is a common method to study the adsorption efficiency of adsorbents. Pseudo-first-order Eq. (7), pseudo-second-order Eq. (8), and Weber-Morris intraparticle diffusion Eq. (9) models were used for the kinetics model fitting of PX adsorption data.

$$\ln q_e - q_t = \ln q_e - k_1 t \quad (7)$$

$$\frac{t}{q_t} = \frac{1}{k_2 q_e^2} + \frac{t}{q_e} \quad (8)$$

$$q_t = k_{id} t^{1/2} + C \quad (9)$$

where q_t (mg/g) and q_e (mg/g) are the concentrations of contaminants on adsorbent at time “ t ” and equilibrium, respectively. k_2 (g/mg•min), k_1 (min⁻¹) and k_{id} (mg/g•min^{1/2}) are second-order model constant, pseudo-first-order model constant, intraparticle diffusion model constant, respectively. t (min) is time and C (mg/g) is boundary layer thickness constant.

2.6.3 Adsorption Isotherms Study

In order to perceive the process of adsorption onto KCS, the experimental results are correlated with the help of isotherm models such as Langmuir Eq. (10), Freundlich Eq. (11), Dubinin-Radushkevich Eqs. (12) and (13).

$$\frac{C_e}{q_e} = \frac{1}{q_m K_L} + \frac{C_e}{q_m} \quad (10)$$

$$\ln q_e = \ln K_F + \frac{1}{n} \ln C_e \quad (11)$$

$$\ln q_e = \ln q_m - B\epsilon^2 \quad (12)$$

$$\epsilon = RT \ln \left(1 + \frac{1}{C_e} \right) \quad (13)$$

where C_e (mg/g) is the equilibrium concentrations of PX and q_e (mg/g) is the adsorption capacity of contaminants in water. K_L (L/mg) is the adsorption equilibrium constant of the Langmuir model; q_m (mg/g) is the maximum adsorption capacity; K_F (mg/g) and n are Freundlich constants related to the adsorption capacity and surface heterogeneity of the adsorbents, respectively. B is a constant related to the mean free energy of adsorption (mol²/J²); ϵ is the Polanyi potential, R (J/(mol•K)) is the gas constant and T (K) is the absolute temperature.

2.6.4 Adsorption Thermodynamics Study

The thermodynamic parameters (Gibbs free energy ΔG^0 , enthalpy ΔH^0 , and entropy ΔS^0) for the adsorption process of PX were conducted at four different temperatures (25°C, 30°C, 35°C and 40°C). The adsorption process is represented by the following Eqs. (14)–(16).

$$\Delta G^0 = -RT \ln K_C \quad (14)$$

$$K_C = \frac{C_A}{C_S} \quad (15)$$

$$\ln(k_c) = \frac{\Delta S^0}{R} - \frac{\Delta H^0}{RT} \quad (16)$$

where ΔG^0 is Gibbs free energy of adsorption, R (J/mol•K) is the gas constant (8.314), T (K) is the absolute temperature and K_c (L/g) is the standard thermodynamic equilibrium constant defined by C_A/C_S , C_A (mg/L) is the concentration of PX adsorbed at the equilibrium and C_S (mg/L) is the concentration of PX that remained at equilibrium.

3 Results and Discussion

3.1 Characterization of Crab Shell Biochar

3.1.1 Porosity Analysis

Fig. 1 shows the N_2 adsorption-desorption isotherms and pore size distributions for CS and KCS. The isotherm of CS showed convex to the p/p_0 axis, which corresponded to a type III isotherm based on IUPAC classification [31]. Accordingly, the adsorbent adsorbate interaction was relatively weak and the adsorbed N_2 molecules were clustered around localized sites on the surface of the suspected nonporous or microporous CS. On the other hand, the isotherm of KCS presented a hysteresis loop at $P/P_0 > 0.4$, and its profile suggested a type IV isotherm [32]. The adsorption capacity increased slowly due to capillary condensation of the suspected mesoporous KCS after multilayer adsorption. Subsequent pore size analysis of KCS using non-local density functional theory (NLDFT) method suggested porosity in the narrow range of 1–15 nm, predominantly mesoporous.

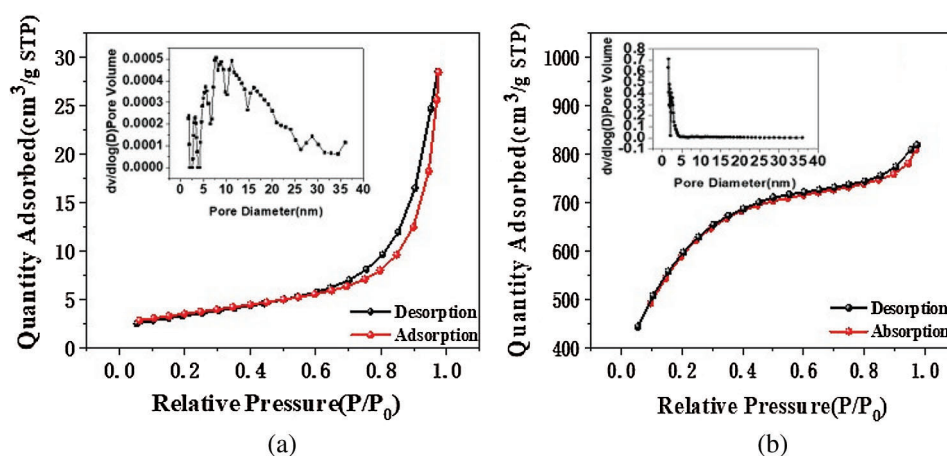


Figure 1: N_2 adsorption-desorption isotherm pore size distributions of CS (a) and KCS (b)

As shown in Tab. 1, the specific surface area and pore volume of CS analyzed from the N_2 adsorption isotherm data were $12 \text{ m}^2/\text{g}$ and $0.04 \text{ cm}^3/\text{g}$. After activation with potassium hydroxide, the specific surface

area and pore volume of KCS increased to 2046 m²/g and 1.15 cm³/g, which were increments of 165 times and 30 times, respectively. This could be due to the removal of the calcium carbonate skeleton of the crab shell upon treatment with hydrochloric acid and subsequently the formation of mesopores upon activation of potassium hydroxide at high temperature. Therefore, the activated crab shell biochar has a significantly high specific surface area as well as high and uniform porosity, which could provide abundant adsorption sites and strongly enhance the adsorption capacity for PX.

Table 1: Specific surface area, pore volume, and average pore size of CS and KCS

Absorbent	Surface area (m ² /g)	Pore volume (cm ³ /g)	Average pore size (nm)
CS powder	12	0.04	3.83
KCS powder	2046	1.15	2.48

3.1.2 Phase Structure Analysis

XRD pattern showed that the crystal structure and phase analysis of CS and KCS (Fig. 2a). The wide diffraction peaks at 23.2°, 29.4°, 36.0°, 39.4°, 43.2°, 47.5°, and 48.5° could be indexed to the (012), (104), (110), (113), (202), (018) and (116) crystal planes of CaCO₃. In addition, there was a diffraction peak at approximately 2θ = 20°, corresponding to (21-2) crystal planes of chitosan. Upon activation with potassium hydroxide, the CaCO₃ peaks disappeared, and only two diffraction peaks located at 20.3° and 43.1° were observed in KCS. These peaks were characteristic of chitosan (21-2) and crystalline graphite (100) planes [33]. The broad weak peak at 2θ = 43.1° further suggested the presence of amorphous carbon.

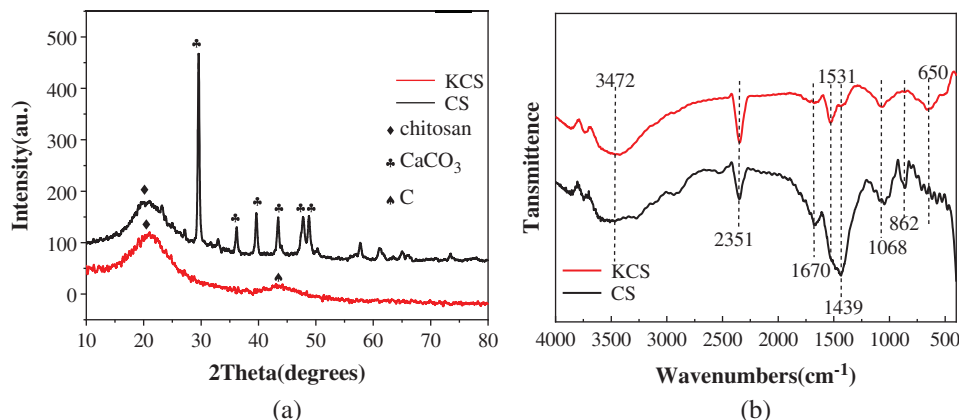


Figure 2: (a) XRD patterns and (b) FTIR spectra of CS and KCS

3.1.3 Surface Functional Group Analysis

FTIR analyses were subsequently carried out to investigate the chemical compositions of CS and KCS surfaces (Fig. 2b). The FTIR spectra of CS and KCS exhibited a broad band at 3250–3750 cm⁻¹ attributed carboxylic acid O–H stretch. The bands at 2830, 2508 cm⁻¹ corresponded to asymmetric and symmetric alkyl –CH stretch. A signal at 2351 cm⁻¹ was due to RH=C=N stretching mode. The absorption band at 1670 cm⁻¹ in CS spectrum arose from the axial C=O stretching of acetamido moieties (amide I), which exhibited red-shift to 1531 cm⁻¹ in KCS spectrum associated with the C=O stretching of amide II [34]. The adsorption band at 1068 cm⁻¹ was due to C–O stretching mode of the glycosidic ring [35]. In addition, the adsorption bands at 1439 and 862 cm⁻¹ were characteristic peaks of calcite [36], which disappeared in KCS spectrum due to the pyrolysis process. Instead, an adsorption peak at 650 cm⁻¹ was present in KCS

spectrum due to O–H bending. The presence of characteristic peaks of chitin in the FTIR spectra of CS and KCS was consistent with their XRD patterns. The types of functional groups present on the surface of biochar strongly dictate its adsorption performance. The methyl-modified surface has been reported to demonstrate excellent adsorption performance for PX [37]. With CS and KCS, the presence of oxygen-containing functional groups such as –OH and C=O alongside alkyl functional groups, which could serve as potential adsorption sites was expected to bestow improved performance for the adsorption for PX [38].

3.1.4 Morphology Analysis

The surface morphologies of CS and KCS were subsequently analyzed with SEM (Fig. 3). The microstructure of CS showed a typical loose layered surface with an uneven arrangement. Upon activation with potassium hydroxide, the surface of KCS exhibited a stratified porous structure with uniform mesopores. In addition, the etching effect of potassium hydroxide on surface structures also resulted in the presence of depressions, dents, and cracks, which increased the overall surface area of KCS [39]. The multi-hierarchical surface of KCS could potentially enhance the adsorption for PX.

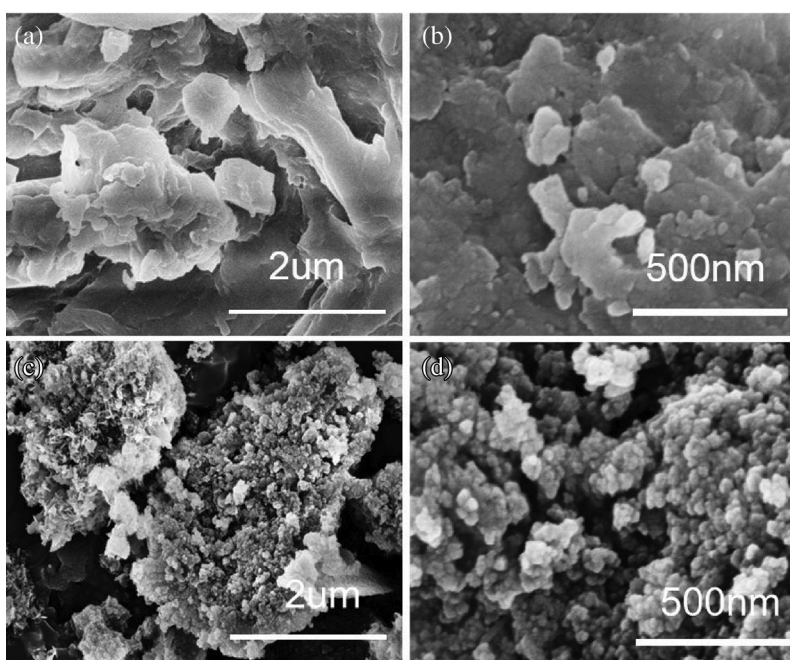


Figure 3: SEM images of CS (a, b) and KCS powders (c, d)

3.2 Study on Adsorption Performance of PX

3.2.1 Effect of Different Initial Concentrations of PX

Fig. 4a shows the adsorption capacity of KCS to different initial concentrations of PX. It was observed that as the concentration of PX in solution increased from 10 to 80 mg/L, the adsorption capacity of KCS increased from 44 to 393 mg/g. However, a further increment of PX concentration beyond 80 mg/L did not result in an increase of adsorption capacity of KCS, which suggested that KCS has reached its equilibrium adsorption capacity. Hence, subsequent experiments were conducted using PX at a concentration of 80 mg/L.

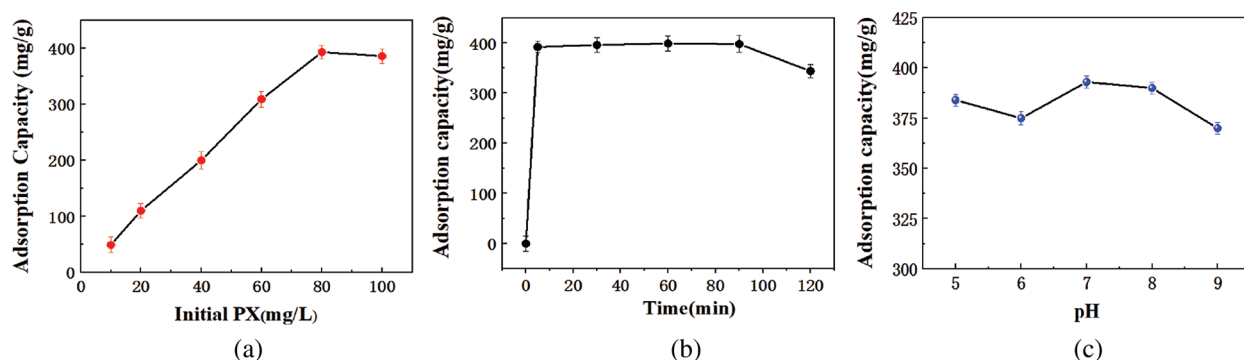


Figure 4: Effect of various factors on adsorption capacity of KCS for PX: (a) initial PX concentration, (b) adsorption time, (c) solution pH

3.2.2 Effect of Adsorption Time

Fig. 4b illustrates the effect of adsorption time on the adsorption capacity of KCS for PX. The adsorption efficiency increased with increasing adsorption time for KCS until equilibrium is attained, and the maximum adsorption capacity of 390 mg/g was attained within 5 min and with a removal rate of up to 97.5% PX. The maximum adsorption capacity retained for the subsequent 85 min before it decreased after 90 min of exposure. This could be attributed to the desorption of PX from KCS due to competitive adsorption by water molecules. The initial high adsorption efficiency of KCS for PX could be due to an abundance of active sites available on the surface of KCS, as seen from earlier FTIR analysis. As a result, the adsorption equilibrium was attained within such a short time [9,40]. In addition, the low solubility of PX in aqueous solution and the hydrophobicity of PX could also promote its adsorption to KCS surface via hydrophobic interactions.

3.2.3 Effect of pH

As the surface of KCS contained various functional groups, the pH of the solution would inevitably affect the extent of active sites available for adsorption process. Fig. 4c illustrates the adsorption capacity of KCS for PX in aqueous solutions of pH 5 to 9. The adsorption capacity of KCS for PX was at the highest at 393 mg/g at pH 7. In acidic conditions, because of the high concentration of the competitive H^+ in solutions, the protonation of functional groups in the adsorbents made the number of available functional groups decreased, and rendering less effective binding sites for PX [9]. In alkaline conditions, deprotonated functional groups could exert electrostatic repulsion, and thus reduced the adsorption efficiency [41]. In addition, the surface groups ($-COOH$) was essential for the binding of hydrophobic contaminants and the pH of the solution will be protonated and deprotonated by organic compounds. As for the neutral condition, the interactions of negatively charged oxygen-bearing functional groups on KCS and positively charged π electrons of ring structures could cause strong electrostatic interactions through which the adsorption capacity was increased [42]. This result indicated that the electrostatic interaction was involved in the adsorption process.

3.2.4 Adsorption Kinetics Study

Fig. 5 indicates the fitting of experimental data with the respective kinetics models for PX. Tab. 2 provides the results of the kinetics model fittings for the adsorption of PX on KCS. It can be observed that the pseudo-second-order model showed the highest R^2 value of 0.980, as compared to the pseudo-first-order with an R^2 value of 0.862, and the Weber-Morris intraparticle diffusion model with an R^2 value of 0.870. Hence, the pseudo-second-order model was the best model to describe the adsorption of PX on KCS. Based on the least-squares regression, the obtained adsorption amount at equilibrium was

387 mg/g, which was in good agreement with the experimental data of 393 mg/g. In accordance with the pseudo-second-order kinetics mechanism, the adsorption's mechanism is chemically rate-controlling, which incorporates the valence forces by sharing or exchanging electrons between adsorbent and adsorbate [9]. Besides, it was also noted that the least-squares regression analysis on the intraparticle diffusion model provided a line that did not pass through the origin, implying that intraparticle diffusion was not the sole rate controlling adsorption process. Therefore, the overall adsorption kinetics might also be dependent on diffusion across the boundary layer, in addition to intraparticle diffusion [4].

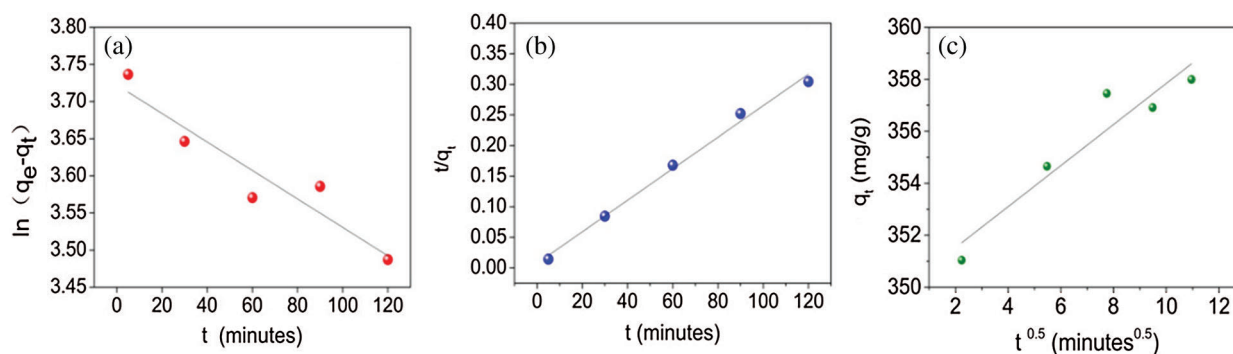


Figure 5: Adsorption kinetics model fitting using (a) pseudo-first-order, (b) pseudo-second-order, and (c) Weber-Morris intraparticle diffusion model for PX

Table 2: Kinetic model parameters for PX adsorption adsorbed by KCS

Model	Parameters	PX
Pseudo-first-order	q_e (mg/g)	41
	k_1 (min^{-1})	0.019
	R^2	0.862
Pseudo-second-order	q_e (mg/g)	387
	k_2 ($\text{g/mg}\cdot\text{min}$) $\times 10^{-4}$	8.86
	R^2	0.980
Intraparticle diffusion model	C (mg/g)	350
	K_{id} ($\text{mg/g}\cdot\text{min}^{1/2}$)	0.790
	R^2	0.870

3.2.5 Adsorption Isotherms Study

Fig. 6 indicates the fitting of data with isotherm models while adsorption parameters and regression data of the models are calculated and presented in Tab. 3. The regression coefficient (R^2) of the Freundlich model has the highest value for the adsorption of PX on KCS, indicating that the Freundlich equation is more suited for describing the adsorption of PX on KCS and the adsorption process is multilayer adsorption. The value of n was close to 1, which indicated favorable adsorption of PX to KCS.

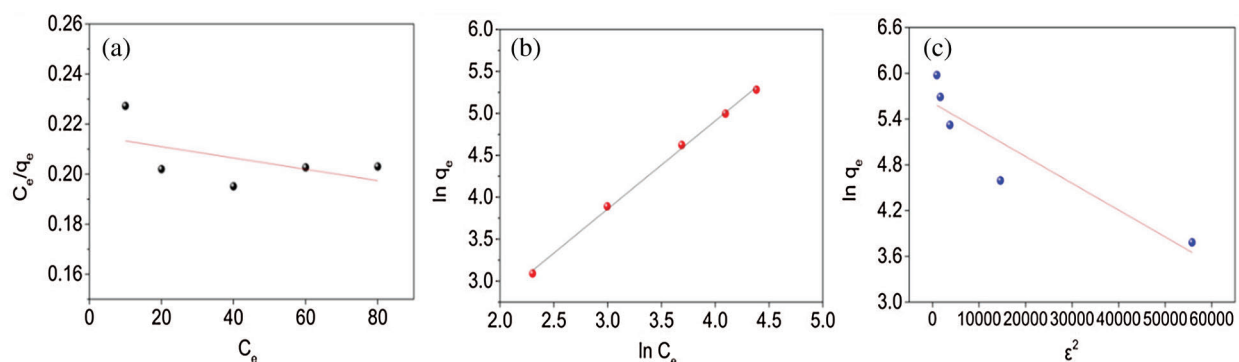


Figure 6: Adsorption isotherm model fittings using (a) Langmuir, (b) Freundlich, and (c) Dubinin-Radushkevich models for PX

Table 3: Isotherm models parameters for PX adsorption adsorbed by KCS

Model	Parameters	PX
Langmuir	Q_{\max} (mg/g)	442
	K_L (L/mg)	1.05
	R^2	0.037
Freundlich	K_F (mg/g)	2.03
	$1/n$	1.051
	R^2	0.998
Dubinin-Radushkevich	B (mol ² J ²)	3.518×10^{-5}
	Q_m (mg/g)	274.2
	R^2	0.472

3.2.6 Adsorption Thermodynamics Study

By plotting a graph of $\ln Kc$ vs. $1/T$ as illustrated in Fig. 7, the values ΔH° and ΔS° can be estimated from the slopes and intercepts. The thermodynamic parameters are shown in Tab. 4. The obtained ΔH° value was negative, which indicated the exothermic nature of PX adsorption onto KCS. Meanwhile, the ΔS° was negative, indicating that the entropy of the system decreased during the adsorption process. This result indicated that PX adsorption by the KCS was slightly temperature-dependent. As listed in Tab. 2, the values ΔG° turned out to be -12.26 , -11.97 , -11.67 and -11.37 kJ/mol at 298, 303, 308 and 313 K, respectively. Besides, the negative values of ΔG° indicated that the PX adsorption process on KCS was spontaneous and increasing the temperature would decrease the adsorption capability of KCS. Similar results have been presented by Yu et al. [43].

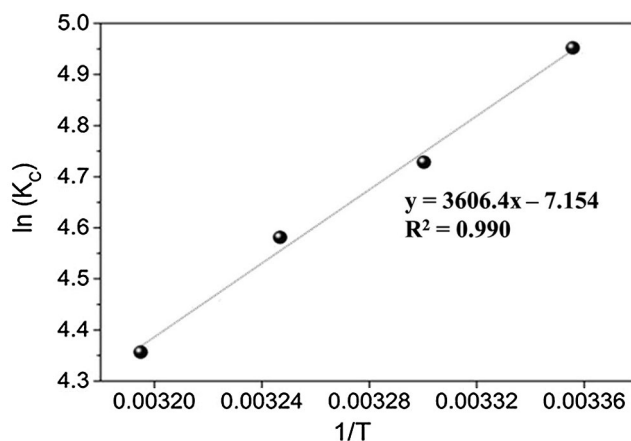


Figure 7: A plot of $\ln K_c$ vs. $1/T$ for adsorption of PX on KCS at various temperatures from 298 to 313 K

Table 4: Thermodynamic parameters of PX adsorption on KCS at different temperatures

T	$\Delta G^\circ/\text{kJ/mol}$	$\Delta H^\circ/\text{kJ/mol}$	$\Delta S^\circ/\text{J/mol}\cdot\text{K}$
298	-12.26	-29.99	-59.48
303	-11.97		
308	-11.67		
313	-11.37		

3.3 Comparison with Other Adsorbents

In order to evaluate the performance of KCS correctly, its performance was compared with the PX adsorption performance reported in other literatures. Tab. 5 shows a comparison of the maximum adsorption capacities of various adsorbents for PX. KCS attained the highest adsorption capacity at 393 mg/g when compared against other previously reported adsorbents. The high adsorption rate of PX on KCS upon initial contact could be attributed to the availability of more active sites and the high surface area of KCS for interaction with PX molecules. Biomass-based biochar has the advantages of high specific surface area, multi-layer porous nanostructure, availability and easy functionalization, which is an ideal material for the construction of high-efficiency adsorbents for adsorption of environmental pollutants [25,26,28]. The methyl and oxygen-containing functional groups on the surface of KCS have also contributed to its better adsorption properties for PX [37]. Through surface modification, the specific surface area and porosity can be increased, which is more conducive to the adsorption of PX [44–46]. Adsorption properties of ethylbenzene and xylene isomers by activated-MWCNTs have been found to depend significantly on mesopore volumes and hydroxyl groups [47]. Hydrophobic surface of ACFs (Six activated carbon fibers) was one of main factors influencing the adsorption, more hydrophobic micropore surface chemistry and high carbon content have the higher adsorption of BTEX [48]. In addition, the low solubility of PX in aqueous solution and hydrophobicity of PX were conducive for the binding of PX to the surface of KCS via hydrophobic interactions. Furthermore, crab shells as a by-product of seafood products could be easily obtained at a much lower cost than carbon nanotube or organosilica while eventually add value to global waste management efforts when exploited as starting material for biochar.

Table 5: Comparison of adsorption capacity of different adsorbents for PX removal

Adsorbent	PX q_{\max} (mg/g)	BET surface area(m ² /g)	Reference
Mesoporous silica nanoparticle	238	255	[11]
Modified periodic mesoporous organosilica	0.63	484	[44]
Smectite organoclay	0.75	61	[45]
Activated carbon	269	871	[46]
SWCNTs (HNO ₃)	85	284	[37]
MWCN (KOH)	96	534	[47]
Six activated carbon fibers	185	483	[48]
KCS	393	2046	This work

4 Conclusions

In this work, activated biochar derived from crab shell was synthesized, characterized, and studied for its adsorption efficiency for PX removal from aqueous solution. The activated biochar KCS, demonstrated the highest adsorption capacity for PX at 393 mg/g, as compared to other adsorbents reported so far. The performance of KCS was attributed to its high specific surface area, hierarchical porous nanostructure, and an abundance of active sites, i.e., lipophilic functional groups, such as methyl and oxygen-containing functional groups, on its surface to aid effective adsorption of PX. Further adsorption kinetic study illustrated that the present adsorption process followed the pseudo-second-order model, while it was inferred from adsorption isotherm analysis that the Freundlich isotherm model fitted the data appropriately well. Consequently, the inexpensive activated crab shell biochar is expected to contribute significantly towards environmental remediation efforts.

Funding Statement: This study was supported by the Natural Science Foundation of Zhejiang Province of China (No. LQ16D060004), Key Research and Development Projects of Zhejiang Province of China (No. 2018C02043), Demonstration Project of Marine Economic Innovation and Development of Zhoushan City of China, and Demonstration Project of Marine Economic Innovation and Development of Yantai City of China (No. YHCX-SW-L-201705).

Conflicts of Interest: The authors declare that they have no conflicts of interest to report regarding the present study.

References

1. Dai, T., Li, C. Z., Li, L., Zhao, Z. K., Zhang, B. et al. (2018). Selective production of renewable para-xylene via tungsten carbide-catalyzed atom-economic cascade reactions. *Angewandte Chemie*, 130, 1826–1830. DOI 10.1002/ange.201710074.
2. Jahn, M. K., Haderlein, S. B., Meckenstock, R. U. (2015). Anaerobic degradation of benzene, toluene, ethylbenzene, and o-xylene in sediment-free iron-reducing enrichment cultures. *Applied and Environmental Microbiology*, 71, 3355–3358. DOI 10.1128/AEM.71.6.3355-3358.2005.
3. Maneffa, A., Pricel, P., Lopez-Sanchez, J. A. (2016). Biomass-derived renewable aromatics: Selective routes and outlook for p-xylene commercialisation. *ChemSusChem*, 9, 2736–2748. DOI 10.1002/cssc.201600605.
4. Abbas, A., Abussaud, B. A., Al-Baghli, N. A., Redhwi, H. H. (2017). Adsorption of toluene and paraxylene from aqueous solution using pure and iron oxide impregnated carbon nanotubes: Kinetics and isotherms study. *Bioinorganic Chemistry & Applications*, 2017, 1–11. DOI 10.1155/2017/2853925.

5. Liu, C., Long, Y. H., Wang, Z. B. (2018). Optimization of conditions for preparation of ZSM-5@ silicalite-1 core-shell catalysts via hydro-thermal synthesis. *Chinese Journal of Chemical Engineering*, 26, 2070–2076. DOI 10.1016/j.cjche.2018.03.030.
6. Liu, W. J., Jiang, H., Yu, H. Q. (2015). Development of biochar-based functional materials: Toward a sustainable platform carbon material. *Chemical Reviews*, 115, 12251–12285. DOI 10.1021/acs.chemrev.5b00195.
7. Wang, L., He, H., Zhang, C. B., Wang, Y. F., Zhang, B. (2016). Effects of precursors for manganese-loaded γ -Al₂O₃ catalysts on plasma-catalytic removal of o-xylene. *Chemical Engineering Journal*, 288, 406–413. DOI 10.1016/j.cej.2015.12.023.
8. Chen, Y. G., Ye, W. M., Xie, Z. J., Chen, B., Cui, Y. J. (2012). Remediation of saturated shanghai sandy silt contaminated with p-xylene using air sparging. *Natural Hazards*, 62, 1005–1020. DOI 10.1007/s11069-012-0129-1.
9. Anjum, H., Johari, K., Gnanasundaram, N., Appusamy, A., Thanabalan, M. (2019). Investigation of green functionalization of multi-walled carbon nanotubes and its application in adsorption of benzene, toluene & p-xylene from aqueous solution. *Journal of Cleaner Production*, 221, 323–338. DOI 10.1016/j.jclepro.2019.02.233.
10. Ramteke, L. P., Gogate, P. R. (2016). Removal of benzene, toluene and xylene (BTX) from wastewater using immobilized modified prepared activated sludge (MPAS). *Journal of Chemical Technology & Biotechnology*, 91, 456–466. DOI 10.1002/jctb.4599.
11. Kim, S., Park, J., Lee, C. (2013). Surface-functionalized mesoporous silica nanoparticles as sorbents for BTEX. *Journal of Porous Material*, 20, 1087–1093. DOI 10.1007/s10934-013-9690-6.
12. Lu, C. Y., Su, F. S., Hu, S. K. (2008). Surface modification of carbon nanotubes for enhancing BTEX adsorption from aqueous solutions. *Applied Surface Science*, 254, 7035–7041. DOI 10.1016/j.apsusc.2008.05.282.
13. Al-Qodah, Z. (2006). Biosorption of heavy metal ions from aqueous solutions by activated sludge. *Desalination*, 196, 164–176. DOI 10.1016/j.desal.2005.12.012.
14. Alpatova, A. L., Shan, W., Babica, P., Upham, B. L., Rogensues, A. R. et al. (2010). Single-walled carbon nanotubes dispersed in aqueous media via non-covalent functionalization: Effect of dispersant on the stability, cytotoxicity, and epigenetic toxicity of nanotube suspensions. *Water Research*, 44, 505–520. DOI 10.1016/j.watres.2009.09.042.
15. Yao, X. X., Ji, L. L., Guo, J., Ge, S. L., Lu, W. C. et al. (2020). An abundant porous biochar material derived from wakame (*Undaria pinnatifida*) with high adsorption performance for three organic dyes-scienceDirect. *Bioresource Technology*, 318. DOI 10.1016/j.biortech.2020.124082.
16. Tang, W., Huang, H., Gao, Y., Liu, X., Yang, X. et al. (2015). Preparation of a novel porous adsorption material from coal slag and its adsorption properties of phenol from aqueous solution. *Materials & Design*, 88, 1191–1200. DOI 10.1016/j.matdes.2015.09.079.
17. Zhou, Y. R., Zhang, H. L., Cai, L., Guo, J., Wang, Y. N. et al. (2018). Preparation and characterization of macroalgae biochar nanomaterials with highly efficient adsorption and photodegradation ability. *Materials*, 11(9), 1709. DOI 10.3390/ma11091709.
18. Mohan, D., Sarswat, A., Yong, S. O. Jr., C.U.P. (2014). Organic and inorganic contaminants removal from water with biochar, a renewable, low cost and sustainable adsorbent—a critical review. *Bioresource Technology*, 160, 191–202. DOI 10.1016/j.biortech.2014.01.120.
19. Guo, J., Song, Y. Q., Ji, X. Y., Ji, L. L., Cai, L. et al. (2019). Preparation and characterization of nanoporous activated carbon derived from prawn shell and its application for removal of heavy metal ions. *Materials*, 12(2), 241. DOI 10.3390/ma12020241.
20. Zheng, C. F., Zheng, H. L., Sun, Y. J., Xu, B., Wang, Y. et al. (2019). Simultaneous adsorption and reduction of hexavalent chromium on the poly(4-vinyl pyridine) decorated magnetic chitosan biopolymer in aqueous solution. *Bioresource Technology*, 293, 122038. DOI 10.1016/j.biortech.2019.122038.
21. Choi, E. J., Jin, H. M., Lee, S. H., Math, R. K., Madsen, E. L. et al. (2013). Comparative genomic analysis and benzene, toluene, ethylbenzene, and o-, m-, and p-xylene (BTEX) degradation pathways of *Pseudoxanthomonas spadix* BD-a59. *Applied & Environmental Microbiology*, 79, 663–671. DOI 10.1128/AEM.02809-12.

22. Walcarius, A., Mercier, L. (2010). Mesoporous organosilica adsorbents: Nanoengineered materials for removal of organic and inorganic pollutants. *Journal of Materials Chemistry*, *20*, 4478–4511. DOI 10.1039/b924316j.
23. Duan, S., Li, L., Zhuang, Z. J., Wu, W. Y., Hong, S. Y. et al. (2012). Improved production of chitin from shrimp waste by fermentation with epiphytic lactic acid bacteria. *Carbohydrate Polymers*, *89*, 1283–1288. DOI 10.1016/j.carbpol.2012.04.051.
24. Fu, M., Chen, W., Zhu, X. X., Yang, B. C., Liu, Q. Y. (2019). Crab shell derived multi-hierarchical carbon materials as a typical recycling of waste for high performance supercapacitors. *Carbon*, *141*, 748–757. DOI 10.1016/j.carbon.2018.10.034.
25. Chen, T., Deng, S. B., Wang, B., Huang, J., Wang, Y. J. et al. (2015). CO₂ adsorption on crab shell derived activated carbons: Contribution of micropores and nitrogen-containing groups. *RSC Advances*, *5*, 48323–48330. DOI 10.1039/C5RA04937G.
26. Gao, Y., Xu, S. P., Yue, Q. Y., Wu, Y. W., Gao, B. Y. (2016). Chemical preparation of crab shell-based activated carbon with superior adsorption performance for dye removal from wastewater. *Journal of the Taiwan Institute of Chemical Engineers*, *61*, 327–335. DOI 10.1016/j.jtice.2015.12.023.
27. Mubarak, N. M., Sahu, J. N., Abdullah, E. C., Jayakumar, N. S. (2016). Rapid adsorption of toxic Pb(II) ions from aqueous solution using multiwall carbon nanotubes synthesized by microwave chemical vapor deposition technique. *Journal of Environmental Sciences*, *45*, 143–155. DOI 10.1016/j.jes.2015.12.025.
28. Arshadi, M., Shakeri, H., Salvacion, J. W. L. (2016). A green adsorbent for the removal of BTEX from aqueous media. *RSC Advances*, *6* (17), 14290–14305. DOI 10.1039/C5RA24757H.
29. Cai, L., Zhang, Y., Zhou, Y. R., Zhang, X. D., Ji, L. L. et al. (2019). Effective adsorption of diesel oil by crab-shell-derived biochar nanomaterials. *Materials*, *12*, 236. DOI 10.3390/ma12020236.
30. Raymundo-Pinero, E., Azais, P., Cacciaguerra, T., Cazorla-Amorós, D., Linares-Solano, A. et al. (2005). KOH and NaOH activation mechanisms of multiwalled carbon nanotubes with different structural organisation. *Carbon*, *43*, 786–795. DOI 10.1016/j.carbon.2004.11.005.
31. Sing, K. S. (1985). Reporting physisorption data for gas/solid systems with special reference to the determination of surface area and porosity (Recommendations 1984). *Pure & Applied Chemistry*, *57*, 603–619. DOI 10.1351/pac198557040603.
32. Shen, J. M., Liu, A. D., Tu, Y., Foo, G. S., Yeo, C. B. et al. (2011). How carboxylic groups improve the performance of single-walled carbon nanotube electrochemical capacitors? *Energy & Environmental Science*, *4*, 4220–4229. DOI 10.1039/c1ee01479j.
33. Arrebola, J. C., Caballero, A., Hernan, L., Morales, J., Marin, M. O. et al. (2010). Improving the performance of biomass-derived carbons in Li-ion batteries by controlling the lithium insertion process. *Journal of the Electrochemical Society*, *157*, A791–A797. DOI 10.1149/1.3425728.
34. Magnacca, G., Guerretta, F., Vizintin, A., Benzi, P., Valsania, M. C. et al. (2018). Preparation, characterization and environmental/electrochemical energy storage testing of low-cost biochar from natural chitin obtained via pyrolysis at mild conditions. *Applied Surface Science*, *427*, 883–893. DOI 10.1016/j.apsusc.2017.07.277.
35. Kumirska, J., Czerwicka, M., Kaczyński, Z., Bychowska, A., Brzozowski, K. et al. (2010). Application of spectroscopic methods for structural analysis of chitin and chitosan. *Marine Drugs*, *8*, 1567–1636. DOI 10.3390/md8051567.
36. Oladoja, N., Raji, I., Olaseni, S., Onimisi, T. (2011). In situ hybridization of waste dyes into growing particles of calcium derivatives synthesized from a gastropod shell (*Achatina achatina*). *Chemical Engineering Journal*, *171*, 941–950. DOI 10.1016/j.cej.2011.04.044.
37. Chin, C. M., Shih, L. C., Tsai, H. J., Liu, T. K. (2007). Adsorption of o-xylene and p-xylene from water by SWCNTs. *Carbon*, *45*, 1254–1260. DOI 10.1016/j.carbon.2007.01.015.
38. Pourzamani, H., Hajizadeh, Y., Fadaei, S. (2015). Efficiency enhancement of multi-walled carbon nanotubes by ozone for benzene removal from aqueous solution. *International Journal of Environmental Health Engineering*, *4*, 29. DOI 10.4103/2277-9183.163972.

39. Jin, H., Hanif, M. U., Capareda, S., Chang, Z. Z., Huang, H. Y. et al. (2016). Copper (II) removal potential from aqueous solution by py-rolysis biochar derived from anaerobically digested algae-dairy-manure and effect of KOH activation. *Journal of Environmental Chemical Engineering*, 4, 365–372. DOI 10.1016/j.jece.2015.11.022.
40. Su, F. S., Lu, C. Y., Hu, S. K. (2010). Adsorption of benzene, toluene, ethylbenzene and p-xylene by NaOCl-oxidized carbon nanotubes. *Colloids and Surfaces a: Physicochemical and Engineering Aspects*, 2010 (353), 83–91. DOI 10.1016/j.colsurfa.2009.10.025.
41. Zhang, L., Xu, T. C., Liu, X. Y., Zhang, Y. Y., Jin, H. J. (2011). Adsorption behavior of multi-walled carbon nanotubes for the removal of olaquinox from aqueous solutions. *Journal of Hazardous Materials*, 197, 389–396. DOI 10.1016/j.jhazmat.2011.09.100.
42. Jankowska, H., Światowski, A., Ościk, J., Kusak, R. (1983). Adsorption from benzene-ethanol binary solutions on activated carbons with different contents of oxygen surface complexes. *Carbon*, 21, 117–120. DOI 10.1016/0008-6223(83)90166-5.
43. Yu, F., Ma, J., Wang, J., Zhang, M. Z., Zheng, J. (2016). Magnetic iron oxide nanoparticles functionalized multi-walled carbon nanotubes for toluene, ethylbenzene and xylene removal from aqueous solution. *Chemosphere*, 146, 162–172. DOI 10.1016/j.chemosphere.2015.12.018.
44. Moura, C. P., Vidal, C. B., Barros, A. L., Costa, L. S., Vasconcellos, L. C. et al. (2011). Adsorption of BTX (benzene, toluene, o-xylene, and p-xylene) from aqueous solutions by modified periodic mesoporous organosilica. *Journal of Colloid & Interface Science*, 363, 626–634. DOI 10.1016/j.jcis.2011.07.054.
45. Carvalho, M., Da Motta, M., Benachour, M., Sales, D., Abreu, C. (2012). Evaluation of BTEX and phenol removal from aqueous solution by multi-solute adsorption onto smectite organoclay. *Journal of Hazardous Materials*, 239, 95–101. DOI 10.1016/j.jhazmat.2012.07.057.
46. Anjum, H., Johari, K., Gnanasundaram, N., Appusamy, A., Thanabalan, M. (2019). Impact of surface modification on adsorptive removal of BTX onto activated carbon. *Journal of Molecular Liquids*, 280, 238–251. DOI 10.1016/j.molliq.2019.02.046.
47. Yu, F., Wu, Y. Q., Ma, J. (2012). Influence of the pore structure and surface chemistry on adsorption of ethylbenzene and xylene isomers by KOH-activated multi-walled carbon nanotubes. *Journal of Hazardous Materials*, 237, 102–109. DOI 10.1016/j.jhazmat.2012.07.059.
48. Mangun, C. L., Yue, Z., Economy, J., Maloney, S., Kemme, P. (2001). Adsorption of organic contaminants from water using tailored ACFs. *Chemistry of Materials*, 13, 2356–2360. DOI 10.1021/cm000880g.